

Neutron-diffraction study of deuterium gas in the critical region

M. Zoppi

*Consiglio Nazionale delle Ricerche, Istituto di Elettronica Quantistica, via Panciatichi 56/30,
I-50127 Firenze, Italy*

R. Magli

Università degli Studi di Firenze, Dipartimento di Energetica, via di S. Marta, I-50139 Firenze, Italy

W. S. Howells and A. K. Soper

Neutron Science Division, Rutherford Appleton Laboratory, Chilton, Didcot, Oxon, OX11 0QX, United Kingdom

(Received 17 October 1988)

The structure factors $S(Q)$ for gaseous deuterium at densities and temperatures in the critical region have been measured for the first time using time-of-flight neutron diffraction at the ISIS pulsed neutron source. The data, when inverted to real space, determine the site-site radial distribution function of the nuclei in the sample. The experimental results are compared with a classical Monte Carlo simulation of a monoatomic Lennard-Jones fluid under equivalent conditions. After correcting for the effects of the molecular form factor in modifying the static structure factor, the simulations reproduce the qualitative trends of the data with density and temperature, with quite good quantitative agreement as well. No evidence is found for the enhanced ordering near the critical point which had previously been predicted from Raman scattering data.

I. INTRODUCTION

There has been renewed interest in the experimental determination of the static structure factor $S(Q)$ for simple monatomic gases in recent times because it has become evident that irreducible many-body forces play an important role in determining correctly the microscopic and macroscopic properties of condensed systems in general and of fluids in particular.¹⁻³ In many practical cases of interest, however, the fluid in question is not a simple noble-gas fluid, but is more likely to be polyatomic, with a good chance that hydrogen or other light atoms are incorporated in the molecular structure. It is important to know the influence of many-body forces in these systems as well, but for molecules with light atoms the corrections due to these many-body effects can be masked by quantum effects associated with the increased size of the molecular wave packet. Until recently, this would have been a rather difficult problem to analyze theoretically because the methods used to interpret experimental data on fluids have been essentially classical in origin. In recent years, however, some simulation results have appeared in which the problem of correcting equilibrium statistical properties for quantum effects has been tackled and the results seem quite promising, in particular for the correction of the radial distribution function (RDF) of gases and liquids.⁴⁻¹¹

One of the methods which is currently used for evaluating quantum corrections of the equilibrium distribution functions uses the Wigner-Kirkwood (WK) approach of expanding quantum properties in terms of \hbar , Planck's constant, combined with classical simulations of fluids.^{8,9,11} This method, which would be exact if it were possible to evaluate all the coefficients in the \hbar expansion,

has been extended to the sixth power in \hbar , allowing a fair determination of quantum corrections for moderately quantum systems such as liquid neon,⁹ which was modeled by the simple 6-12 Lennard-Jones (LJ) intermolecular potential. An advantage of using the WK expansion is that, by analyzing the magnitude of the successive correction terms, the convergence of the asymptotic expansion can be assessed accurately. However for liquid helium where quantum effects are large the WK method diverges at short distances and so the alternative path-integral Monte Carlo (PIMC) technique is used instead.⁶ Unfortunately, while the WK method diverges for He the quantum corrections for Ne are so small that the comparison with the PIMC results for neon is not efficient. Data is needed therefore for an intermediate system so that the two approaches to the problem of quantum corrections can be compared with experimental results.

Molecular hydrogens are interesting systems from this point of view. Their quantum parameters¹¹ are intermediate between those of He and Ne and therefore these systems may play an important role for comparing efficiently the two methods. In particular, for deuterium, the reduced Planck constant Λ^* seems to be about right for complete convergence of the WK series for the pair distribution function, over almost all the physically important distance range, while the corrections are large enough that a comparison between the different methods of calculation becomes practical.¹¹ A second, non-negligible reason to choose molecular deuterium as the experimental system to measure a reasonably quantum RDF, resides in the fact that its coherent cross section for thermal neutrons is much larger than the incoherent cross section. This makes it an almost routine task to measure the structure factor $S(Q)$ for deuterium using

neutrons.

The interest in the case of deuterium was spurred on by the recent discovery of an unexpected fine structure, in the Raman vibrational transitions ($\nu=0\rightarrow 1$, $J=0$) and ($\nu=0\rightarrow 1$, $J=1$) when the gas was near the critical conditions.¹² The expected broadening of the Raman lines was accompanied by the appearance of a regular fine structure, of periodicity close to 6 GHz, which was absent in the case of hydrogen. The origin of this effect is not understood, but one of the proposed causes was that the gas becomes unduly structured at the critical point and that the pair correlation function should show this structure at the nearest-neighbor positions. In particular, it was indicated that the near-neighbor coordination number at the critical density should be close to 8, that the observed effect is bound to integer steps in this coordination number, and that the ordering was a characteristic of the equilibrium fluid. No exhaustive explanation of why the effect should be so large for deuterium but below the limit of detectability for hydrogen was given. However, the principal conclusion was that the effect should be accompanied by an unusual excess structuring of the fluid. Such structuring should be readily discernible by neutron diffraction, although until the present measurements no experimental data were available on deuterium gas in the critical region.

The object of the experiment was therefore to obtain, by neutron diffraction, the structure of deuterium gas at densities and temperatures close to critical conditions. In this thermodynamic region the density is so low that the deBroglie wavelength is much smaller than the average intermolecular distance, so that quantum exchange effects are negligible, while quantum diffraction is large enough to play an important role in determining the radial structure of the fluid. Of course, a neutron experiment of this kind measures the atom-atom correlation function, which must be distinguished from the molecular center-of-mass correlation function. Even so, any enhanced ordering which may be present in the center-center correlation function should also be apparent from the site-site term. A preliminary account of these measurements has already been presented.¹³ In the following a more detailed account of the experiment is given.

In this paper we will limit the discussion to the experimental results for the static structure factor $S(Q)$ and to a comparison with some simple classical simulations. Quantitative comparisons with approximate quantum calculations, which are much more involved and outside the scope of the present work, will be given in a subsequent paper. The experiment is described in Sec. II, while the data analysis and the results for the structure factors and the experimental RDF are presented in Secs. III and IV, respectively. In Sec. V the results of a classical Monte Carlo simulation for a monatomic system are presented, and the correction procedure, to derive the molecular term, is reported in Sec. VI. The conclusion is given in Sec. VII.

II. EXPERIMENT

The diffraction data were measured on the Liquid and Amorphous Diffractometer (LAD) at ISIS, the spallation

neutron source of Rutherford Appleton Laboratory, U.K. This is a time-of-flight diffractometer, incident flight path 10 m, scattered flight path 1 m, with ^3He detectors at scattering angles of 5° , 10° , 20° , 35° , 58° , 90° , and 145° . The neutron collimator converges the beam, $80\times 80\text{ mm}^2$ at source to $10\times 40\text{ mm}^2$ at the sample position. An empty container run was performed at the beginning and at the end of the 61 h of measuring time, to test the stability of the instrumentation, and a background run concluded the experiment.

The cylindrical pressure vessel (inner diameter 19.5 mm, height 60 mm, and wall thickness 0.5 mm) used to contain the sample was manufactured from vanadium sheet, using electron beam welding, by the Institut für Kerntechnik und Energiewandlung, Stuttgart. The top and bottom stainless steel flanges were fitted to the vanadium wall by the same welding technique. A schematic drawing of the container is shown in Fig. 1. The vessel was pressure tested to 100 bar with a change in diameter of less than 0.2%, in agreement with the elastic constant of the material. The cell was mounted on the cold finger of a helium closed-cycle refrigerator and the top and bottom flanges were carefully screened with cadmium sheets (about 2 mm thickness) to avoid any spurious scattering from the steel part of the container. A radiation shield of aluminum with vanadium windows in the neutron path was fitted to the cold head. The temperature was monitored by two calibrated Rh-Fe resistance thermometers located in the top and bottom flanges. When the cell was tested empty at 40 K, a temperature difference of 1.0 K was measured between the two sensors which was due to

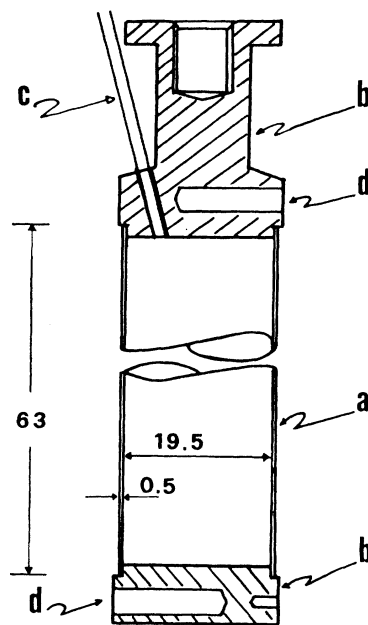


FIG. 1. Schematic drawing of the vanadium scattering container. *a*, vanadium wall; *b*, stainless steel top and bottom flanges; *c*, stainless steel capillary tube; *d*, housing for temperature sensor. Top and bottom flanges have been electron-beam welded to the vanadium wall. Dimensions are given in mm.

TABLE I. Summary of the experimental thermodynamic conditions for the experiment on gaseous deuterium. The critical parameters are $T_c = 38.34$ K, $P_c = 16.65$ bar, and $\rho_c = 10.43$ molecules/nm³ (Ref. 9). The column for $S(Q=0)$ has been evaluated from the hydrogen PVT data of Ref. 14 which were scaled on the critical parameters of deuterium.

Label	T (K)	P (bar)	ρ (molecules/nm ³)	T/T_c	ρ/ρ_c	$S(Q=0)$
<i>a</i>	46.55	33.2	9.6	1.214	0.919	3.92
<i>b</i>	41.8	20.9	7.9	1.090	0.756	5.79
<i>c</i>	41.8	23.2	10.5	1.090	1.005	7.09
<i>d</i>	41.8	27.0	13.6	1.090	1.302	3.41

the low thermal conductivity of the vanadium. This difference was reduced to 0.6 K by wrapping a single layer of extra thin aluminum foil (≈ 6 μm thickness) around the cell. The contribution to the scattering of this foil was estimated to be only 0.3% of the scattering from the vanadium walls.

Deuterium entered the container through a 1.5-m-long stainless steel capillary (inner diameter 0.5 mm) that connected the scattering cell with the gas handling system, composed of a storage bottle, a Bourdon pressure gauge (accuracy 0.1%), and a buffer volume (500 cm³) needed for safety purposes. Three different thermodynamic states were measured along the $T = 41.8$ K isotherm and a fourth one at $T = 46.55$ K. The pressure was set at 20.9, 23.2, and 27.0 bar, respectively, for the lower-temperature runs and to 33.2 bar for the higher temperature. Because of a lack published PVT data for gaseous deuterium we have estimated the densities of the samples by scaling PVT data for hydrogen¹⁴ with the critical parameters for deuterium. Table I summarizes the thermodynamical conditions of the experiment. During the preparation of the experiment the bottom thermal sensor gave a temperature reading greater than the top sensor by 0.4 K with the cell filled with deuterium. However, during the neutron runs the temperature difference was in the range 1.5–2.0 K most likely because of a loss of vacuum in the tank around the sample. The above reported temperatures refer to the upper sensor which was used as the input to the temperature controller. We assumed the upper sensor reading to be correct because estimates of the density based on this sensor were in good agreement with estimates obtained from the analysis of the neutron transmission data for each sample. Therefore, in spite of the good stability of pressure (0.3%) and temperature (0.1%), the accuracy on the absolute value of the density is quite poor and may be affected by a systematic error whose upper limit is estimated of the order of 10%. However, this accuracy is sufficient to ensure that with the specified pressures and temperatures we have spanned the critical density region correctly.

III. DATA ANALYSIS

It is well known that neutron-diffraction data from light atoms will suffer from substantial inelasticity corrections, associated with the nuclear recoil. This effect is most pronounced at large scattering angles when the incident neutron energy needed for a given value of Q is comparable to the energy of the likely inelastic excita-

tions: at small scattering angles the incident neutron energy is much larger than the energy of the excitations and so the recoil correction is small. We have attempted to estimate the inelasticity correction using the method of Egelstaff and Soper.¹⁵ For the time-of-flight case the integral to be solved is

$$\Sigma(Q_e) = \int_{-\infty}^{\infty} d\omega (k_f/k_i) S(Q, \omega) I(k_i) E(k_f) (\partial k_i / \partial k_e)_\omega, \quad (1)$$

where the integral is evaluated for constant neutron time of flight. Here $\Sigma(Q_e)$ is the estimated differential cross section measured as a function of the elastic momentum transfer Q_e ; $h\omega$ is the energy transfer; k_f , k_i , and k_e are the incident, final, and elastic neutron wave vectors, respectively; $S(Q, \omega)$ is the dynamic structure factor; $I(k_i)$ is the incident neutron spectrum; $E(k_f)$ is the detector efficiency function; and the Jacobian arises from the time-of-flight condition which restricts the available incident and final neutron energies to those which satisfy a particular time of arrival at the detector. In the present case where useful data are available to a Q of at least 25 \AA^{-1} the dynamic structure factor must be specified for energy transfers exceeding 1000 meV if the correction is to be evaluated accurately. Unfortunately, the available models for any molecule and deuterium in particular^{16,17} do not apply to such large Q and ω values because they do not incorporate correctly the effects of the rotational-vibrational coupling, and our attempts to evaluate the inelasticity correction (including the interference correction to the single-molecule terms) have not been successful for large scattering angles. Figure 2 shows the estimated correction assuming free deuterium atoms at a temperature of 42 K. It will be seen that the correction is severe at most scattering angles, but for angles below 20° it is on the order of 1–2%. Since this is the level of accuracy of the differential cross sections we have assumed the correction to the low-angle data to be negligible. Therefore the analysis has centered only on the data from 5°, 10°, and 20° scattering angles.

The time-of-flight diffraction data were normalized to the scattering from the empty vanadium pressure cell, to remove the effects of the incident neutron spectrum and detector efficiency, and then corrected for attenuation, multiple scattering, and container scattering in the usual way.¹⁸ Figure 3 shows the measured differential scattering cross sections at 5°, 10°, and 20° scattering angles for all four densities as a function of Q , the momentum transfer. Each curve represents the average of several

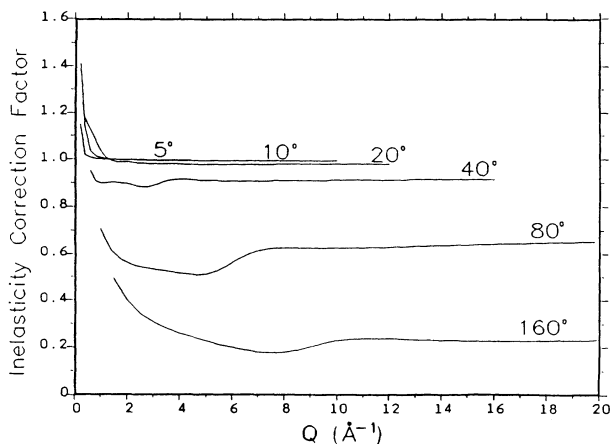


FIG. 2. Inelasticity correction factor calculated for a nucleus of mass $m = 2$ a.u. at $T = 42$ K. The labels indicate the scattering angles of the detectors.

scans. Generally the scans overlapped well, although some variations occurred between detectors, usually at larger scattering angles, which could not be accounted for. Therefore final normalization to remove any residual discrepancies between different scans was achieved by comparison with the expected single-molecule scattering at large- Q values. The data at 5° and 10° scattering angles show the expected enhanced small- Q scattering as determined from the high compressibility of the gas.

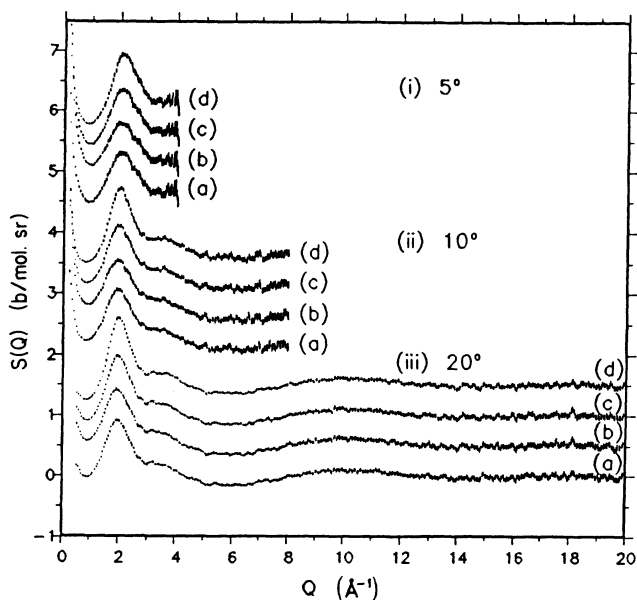


FIG. 3. Fully corrected experimental differential cross sections normalized per molecule for the lowest-angle detector banks on the LAD diffractometer for gaseous deuterium in the critical region. The labels (a), (b), (c), and (d) are defined in Table I. A level of 1.214 b/mol.sr, corresponding to the single-atom scattering has been subtracted from the data prior to plotting.

The final differential cross section for each density was then constructed by means of a weighted average of the data from individual banks, with the raw counts from the calibration runs used as weighting functions.

IV. RESULTS FOR STRUCTURE FACTORS AND PAIR DISTRIBUTION FUNCTION

The site-site structure factors were derived directly from the differential cross sections (ignoring the inelasticity effects as described above) with the simple normalization

$$H(Q) = S(Q) - 1 = [\Sigma(Q_e) - 1.214] / 4b_D^2, \quad (2)$$

where b_D is the deuterium coherent scattering length. The level 1.214 b/mol.sr corresponds to the expected single-atom scattering per molecule. This then gives the structure factor normalized per molecule. The results are shown in Fig. 4 and tabulated in Table II. They show an intermolecular structure peak near $Q = 2 \text{\AA}^{-1}$, and a long-range oscillation at larger- Q values, corresponding to the intramolecular bond distance. The main peak increases monotonically in height with increasing density, but apart from this expected variation there is no sign in $S(Q)$ of any unexpected features, nor is there any evidence for the pronounced structuring at the critical density as predicted by the Raman experiment.

From the experimental $S(Q)$ we have derived the pair correlation function $g(r)$ by means of a direct inversion procedure, described elsewhere,¹⁹ which makes use of a one-dimensional Monte Carlo simulation of the atom-atom distribution functions. Starting from an assumed uniform pair distribution function a new distribution is generated which satisfies the required compressibility constraint [$S(0) = \rho\chi kT$, where ρ is the number density and χ is the isothermal compressibility] and also produces a specified fit to the data, the fit being measured by χ^2 or "R factor," R_f^2 , where

$$R_f^2 = \frac{\sum_Q [S(Q) - M(Q)]^2}{\sum_Q [S(Q)]^2},$$

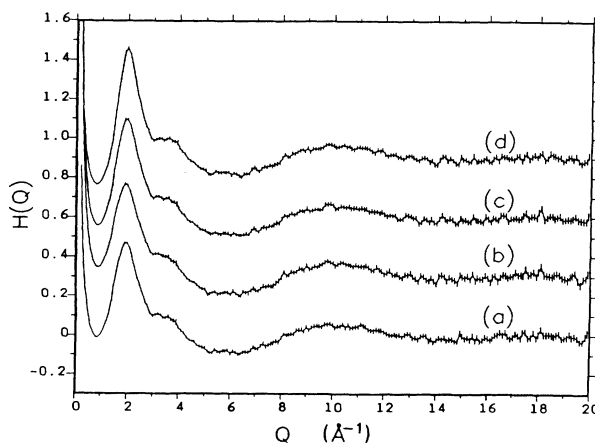


FIG. 4. Experimental structure factors [$H(Q) = S(Q) - 1$] for gaseous deuterium derived from the data of Fig. 3, as described in the text. The labels are defined in Table I.

TABLE II. Experimental $H(Q)=S(Q)-1$ for gaseous deuterium near the critical region. The first number in each column is $H(Q)$ and the second number is the standard deviation. Labels a , b , c , and d correspond to the curves in Figs. 3-5.

Q (Å)	a		b		c		d	
0.2	0.857	0.005	1.412	0.007	1.243	0.006	0.645	0.004
0.3	0.461	0.003	0.735	0.003	0.560	0.003	0.250	0.002
0.4	0.243	0.002	0.404	0.003	0.260	0.002	0.060	0.002
0.5	0.115	0.002	0.225	0.003	0.101	0.002	-0.045	0.002
0.6	0.047	0.002	0.132	0.002	0.024	0.002	-0.098	0.002
0.7	0.010	0.002	0.080	0.002	-0.018	0.002	-0.124	0.002
0.8	-0.010	0.002	0.053	0.002	-0.039	0.002	-0.135	0.002
0.9	-0.009	0.002	0.048	0.002	-0.040	0.002	-0.130	0.002
1.0	0.003	0.002	0.053	0.002	-0.030	0.002	-0.116	0.002
1.1	0.030	0.002	0.079	0.002	-0.003	0.002	-0.087	0.002
1.2	0.067	0.002	0.115	0.003	0.034	0.002	-0.050	0.002
1.3	0.115	0.003	0.161	0.003	0.084	0.003	0.005	0.002
1.4	0.180	0.003	0.218	0.003	0.154	0.003	0.079	0.003
1.5	0.256	0.004	0.289	0.004	0.238	0.003	0.174	0.003
1.6	0.322	0.004	0.346	0.004	0.313	0.004	0.272	0.004
1.7	0.387	0.004	0.402	0.005	0.393	0.004	0.378	0.004
1.8	0.438	0.005	0.441	0.005	0.457	0.005	0.470	0.005
1.9	0.468	0.005	0.468	0.006	0.495	0.005	0.540	0.005
2.0	0.468	0.005	0.459	0.006	0.495	0.006	0.560	0.006
2.1	0.440	0.006	0.430	0.006	0.463	0.006	0.528	0.006
2.2	0.400	0.006	0.392	0.006	0.421	0.006	0.470	0.006
2.3	0.350	0.006	0.353	0.006	0.367	0.006	0.403	0.006
2.4	0.293	0.006	0.296	0.006	0.305	0.006	0.327	0.005
2.5	0.256	0.006	0.260	0.006	0.260	0.006	0.271	0.006
2.6	0.209	0.006	0.218	0.006	0.208	0.006	0.209	0.006
2.7	0.164	0.006	0.174	0.006	0.165	0.006	0.160	0.006
2.8	0.149	0.006	0.159	0.006	0.148	0.006	0.141	0.006
2.9	0.113	0.006	0.124	0.006	0.110	0.006	0.101	0.006
3.0	0.099	0.006	0.112	0.006	0.096	0.006	0.088	0.005
3.1	0.105	0.006	0.115	0.007	0.105	0.006	0.095	0.006
3.2	0.108	0.006	0.113	0.007	0.106	0.006	0.098	0.006
3.3	0.101	0.007	0.107	0.007	0.098	0.007	0.099	0.006
3.4	0.090	0.007	0.102	0.007	0.088	0.007	0.088	0.006
3.5	0.088	0.007	0.099	0.008	0.095	0.007	0.095	0.007
3.6	0.095	0.009	0.009	0.009	0.096	0.009	0.100	0.008
3.7	0.081	0.009	0.083	0.009	0.080	0.009	0.088	0.008
3.8	0.074	0.009	0.076	0.010	0.077	0.009	0.083	0.009
3.9	0.067	0.014	0.068	0.014	0.067	0.013	0.078	0.014
4.0	0.041	0.008	0.045	0.009	0.043	0.008	0.052	0.008
4.1	0.023	0.006	0.028	0.006	0.022	0.006	0.034	0.005
4.2	0.011	0.006	0.012	0.006	0.011	0.006	0.021	0.006
4.3	-0.012	0.006	-0.008	0.006	-0.013	0.006	-0.003	0.005
4.4	-0.023	0.006	-0.018	0.006	-0.022	0.006	-0.015	0.005
4.5	-0.029	0.006	-0.026	0.006	-0.023	0.006	-0.019	0.005
4.6	-0.031	0.006	-0.029	0.007	-0.036	0.006	-0.029	0.006
4.7	-0.049	0.006	-0.042	0.007	-0.045	0.006	-0.043	0.006
4.8	-0.058	0.006	-0.054	0.007	-0.060	0.006	-0.054	0.006
4.9	-0.061	0.007	-0.062	0.008	-0.064	0.007	-0.058	0.007
5.0	-0.064	0.007	-0.064	0.008	-0.068	0.007	-0.061	0.007
5.1	-0.083	0.007	-0.094	0.007	-0.080	0.007	-0.083	0.006
5.2	-0.088	0.007	-0.087	0.007	-0.084	0.007	-0.085	0.006
5.3	-0.088	0.007	-0.082	0.007	-0.082	0.007	-0.079	0.006
5.4	-0.074	0.008	-0.077	0.008	-0.076	0.008	-0.066	0.007
5.5	-0.083	0.007	-0.089	0.008	-0.084	0.007	-0.074	0.007
5.6	-0.086	0.008	-0.086	0.008	-0.089	0.008	0.074	0.007
5.7	-0.080	0.008	-0.083	0.008	-0.081	0.008	-0.073	0.007
5.8	-0.079	0.008	-0.080	0.009	-0.081	0.008	-0.075	0.008
5.9	-0.079	0.008	-0.082	0.009	-0.081	0.008	-0.073	0.008

TABLE II. (Continued).

Q (Å)	a		b		c		d	
6.0	-0.093	0.008	-0.091	0.008	-0.092	0.008	-0.087	0.007
6.1	-0.082	0.008	-0.073	0.009	-0.079	0.008	-0.076	0.007
6.2	-0.088	0.008	-0.086	0.009	-0.087	0.008	-0.081	0.007
6.3	-0.097	0.008	-0.096	0.008	-0.091	0.008	-0.090	0.007
6.4	-0.095	0.008	-0.101	0.008	-0.091	0.008	-0.097	0.007
6.5	-0.086	0.009	-0.076	0.009	-0.087	0.009	-0.081	0.008
6.6	-0.085	0.008	-0.082	0.009	-0.080	0.008	-0.082	0.008
6.7	-0.088	0.009	-0.090	0.009	-0.088	0.009	-0.080	0.008
6.8	-0.075	0.009	-0.070	0.010	-0.066	0.009	-0.057	0.009
6.9	-0.059	0.010	-0.058	0.011	-0.052	0.010	-0.046	0.009
7.0	-0.065	0.009	-0.068	0.010	-0.064	0.009	-0.057	0.009
7.1	-0.069	0.009	-0.073	0.010	-0.074	0.009	-0.069	0.008
7.2	-0.054	0.010	-0.059	0.011	-0.057	0.010	-0.053	0.009
7.3	-0.042	0.011	-0.047	0.012	-0.048	0.011	-0.044	0.010
7.4	-0.057	0.011	-0.052	0.011	-0.054	0.011	-0.047	0.010
7.5	-0.050	0.011	-0.046	0.011	-0.046	0.011	-0.038	0.010
7.6	-0.041	0.011	-0.049	0.012	-0.044	0.011	-0.042	0.010
7.7	-0.038	0.013	-0.045	0.013	-0.038	0.012	-0.032	0.012
7.8	-0.029	0.012	-0.030	0.013	-0.028	0.012	-0.030	0.011
7.9	-0.034	0.012	-0.022	0.013	-0.028	0.012	-0.022	0.011
8.0	-0.012	0.011	-0.003	0.011	-0.007	0.010	0.000	0.010
8.1	0.007	0.009	0.023	0.010	0.010	0.009	0.018	0.008
8.2	0.002	0.009	0.006	0.010	0.005	0.009	0.007	0.008
8.3	0.004	0.009	0.008	0.010	0.012	0.009	0.007	0.008
8.4	0.008	0.009	0.026	0.010	0.020	0.009	0.024	0.009
8.5	0.007	0.009	0.022	0.010	0.014	0.009	0.023	0.009
8.6	0.026	0.010	0.028	0.010	0.020	0.009	0.032	0.009
8.7	0.029	0.010	0.042	0.010	0.033	0.010	0.041	0.009
8.8	0.033	0.010	0.039	0.011	0.034	0.010	0.045	0.009
8.9	0.021	0.010	0.033	0.010	0.030	0.010	0.035	0.009
9.0	0.044	0.010	0.058	0.011	0.045	0.010	0.052	0.009
9.1	0.029	0.010	0.038	0.011	0.030	0.010	0.034	0.009
9.2	0.043	0.010	0.045	0.011	0.037	0.010	0.050	0.009
9.3	0.048	0.010	0.055	0.011	0.043	0.010	0.050	0.010
9.4	0.051	0.010	0.050	0.011	0.044	0.010	0.049	0.010
9.5	0.048	0.011	0.059	0.011	0.039	0.010	0.051	0.010
9.6	0.045	0.011	0.064	0.012	0.044	0.011	0.057	0.010
9.7	0.059	0.011	0.075	0.012	0.068	0.011	0.068	0.010
9.8	0.059	0.011	0.081	0.012	0.066	0.011	0.073	0.010
9.9	0.060	0.011	0.073	0.012	0.070	0.011	0.070	0.010
10.0	0.053	0.011	0.070	0.012	0.063	0.011	0.067	0.010
10.1	0.041	0.011	0.056	0.012	0.044	0.011	0.058	0.010
10.2	0.048	0.011	0.064	0.012	0.048	0.011	0.060	0.010
10.3	0.047	0.011	0.072	0.012	0.057	0.011	0.062	0.010
10.4	0.058	0.012	0.073	0.012	0.055	0.011	0.068	0.011
10.5	0.039	0.011	0.062	0.012	0.050	0.011	0.057	0.011
10.6	0.056	0.012	0.061	0.012	0.056	0.012	0.062	0.011
10.7	0.040	0.011	0.058	0.012	0.046	0.011	0.051	0.011
10.8	0.043	0.012	0.052	0.012	0.049	0.012	0.046	0.011
10.9	0.045	0.012	0.061	0.013	0.052	0.012	0.056	0.011
11.0	0.046	0.012	0.055	0.013	0.045	0.012	0.057	0.011
11.1	0.058	0.012	0.052	0.013	0.049	0.012	0.054	0.011
11.2	0.050	0.012	0.050	0.013	0.043	0.012	0.054	0.011
11.3	0.045	0.012	0.057	0.013	0.044	0.012	0.052	0.011
11.4	0.030	0.012	0.048	0.013	0.028	0.012	0.047	0.011
11.5	0.026	0.012	0.032	0.013	0.034	0.012	0.035	0.011
11.6	0.024	0.012	0.033	0.013	0.031	0.012	0.030	0.011
11.7	0.030	0.012	0.051	0.013	0.032	0.012	0.045	0.011
11.8	0.028	0.012	0.037	0.013	0.024	0.012	0.037	0.011
11.9	0.027	0.012	0.029	0.013	0.029	0.012	0.045	0.012

TABLE II. (Continued).

Q (Å)	a		b		c		d	
12.0	0.019	0.012	0.014	0.013	0.018	0.012	0.023	0.011
12.1	0.010	0.012	0.022	0.013	0.008	0.012	0.011	0.011
12.2	0.005	0.012	0.032	0.013	0.013	0.012	0.020	0.011
12.3	0.003	0.012	0.011	0.013	0.010	0.012	0.018	0.011
12.4	0.009	0.013	0.010	0.013	0.012	0.012	0.021	0.012
12.5	0.001	0.012	0.015	0.013	-0.007	0.012	0.006	0.011
12.6	0.005	0.013	0.002	0.013	-0.007	0.012	0.007	0.011
12.7	-0.006	0.013	-0.006	0.013	-0.006	0.012	-0.004	0.011
12.8	0.004	0.013	0.013	0.014	0.014	0.013	0.009	0.012
12.9	0.010	0.013	0.009	0.014	0.011	0.013	0.013	0.012
13.0	0.006	0.013	0.018	0.014	0.009	0.013	0.013	0.012
13.1	-0.012	0.013	0.001	0.014	-0.001	0.013	0.005	0.012
13.2	-0.008	0.013	-0.007	0.014	0.001	0.013	-0.004	0.012
13.3	-0.017	0.013	-0.020	0.014	-0.027	0.012	-0.009	0.012
13.4	-0.003	0.013	0.010	0.014	-0.022	0.013	0.002	0.012
13.5	0.000	0.013	0.002	0.014	-0.002	0.013	0.004	0.012
13.6	0.000	0.014	-0.012	0.014	-0.009	0.013	0.000	0.012
13.7	-0.026	0.013	-0.019	0.014	-0.022	0.013	-0.017	0.012
13.8	-0.017	0.013	-0.005	0.014	-0.007	0.013	-0.010	0.012
13.9	-0.034	0.013	-0.019	0.014	-0.025	0.013	-0.031	0.012
14.0	-0.020	0.013	-0.033	0.014	-0.028	0.013	-0.031	0.012
14.1	-0.010	0.014	0.006	0.015	-0.006	0.014	-0.006	0.013
14.2	-0.017	0.014	0.011	0.015	0.013	0.014	0.011	0.013
14.3	-0.010	0.014	0.002	0.015	-0.007	0.014	0.009	0.013
14.4	-0.024	0.014	-0.019	0.015	-0.014	0.014	-0.011	0.013
14.5	-0.019	0.014	0.000	0.015	-0.004	0.014	0.002	0.013
14.6	-0.019	0.014	-0.011	0.015	-0.010	0.014	-0.010	0.013
14.7	-0.027	0.014	-0.015	0.015	-0.028	0.014	-0.026	0.013
14.8	-0.028	0.014	-0.029	0.015	-0.026	0.014	-0.029	0.012
14.9	0.016	0.015	0.012	0.015	0.001	0.014	0.010	0.013
15.0	-0.001	0.014	0.002	0.015	-0.013	0.014	-0.004	0.013
15.1	-0.016	0.014	-0.005	0.015	-0.010	0.014	-0.006	0.013
15.2	-0.009	0.015	0.005	0.016	-0.019	0.014	-0.018	0.013
15.3	-0.022	0.014	-0.013	0.016	-0.020	0.014	-0.015	0.013
15.4	-0.002	0.015	0.016	0.016	0.007	0.015	0.012	0.014
15.5	-0.027	0.014	-0.018	0.015	-0.011	0.014	-0.014	0.013
15.6	-0.006	0.015	-0.003	0.016	-0.012	0.015	-0.012	0.014
15.7	-0.030	0.014	-0.010	0.016	-0.017	0.014	-0.011	0.013
15.8	-0.023	0.015	-0.008	0.016	-0.022	0.015	-0.007	0.014
15.9	-0.008	0.015	0.008	0.016	0.008	0.015	0.004	0.014
16.0	-0.013	0.015	-0.006	0.016	-0.005	0.015	-0.014	0.014
16.1	-0.023	0.015	-0.024	0.016	-0.020	0.015	-0.019	0.014
16.2	-0.013	0.015	0.000	0.016	-0.001	0.015	0.000	0.014
16.3	0.003	0.015	0.009	0.017	-0.004	0.015	0.008	0.014
16.4	0.004	0.016	-0.018	0.016	-0.010	0.015	-0.010	0.014
16.5	0.019	0.016	0.001	0.017	0.015	0.016	0.016	0.015
16.6	0.006	0.016	0.013	0.017	0.015	0.016	0.009	0.014
16.7	0.018	0.016	0.010	0.017	0.011	0.016	0.010	0.015
16.8	-0.002	0.015	-0.003	0.016	-0.017	0.015	-0.001	0.014
16.9	-0.014	0.016	0.005	0.017	-0.004	0.016	0.003	0.015
17.0	-0.009	0.016	0.005	0.017	-0.004	0.016	-0.007	0.014
17.1	0.012	0.016	0.026	0.017	0.002	0.016	0.011	0.015
17.2	0.001	0.016	0.011	0.017	-0.004	0.016	0.014	0.015
17.3	-0.010	0.016	0.013	0.017	-0.001	0.016	-0.011	0.014
17.4	0.017	0.016	0.009	0.017	0.015	0.016	0.011	0.015
17.5	0.021	0.017	0.042	0.018	0.025	0.017	0.023	0.016
17.6	-0.011	0.016	0.011	0.017	-0.001	0.016	-0.002	0.015
17.7	-0.007	0.016	0.015	0.018	0.008	0.016	0.010	0.015
17.8	0.015	0.017	0.026	0.018	0.009	0.017	0.019	0.016
17.9	-0.011	0.016	0.005	0.017	0.000	0.016	0.008	0.015

TABLE II. (Continued).

Q (Å)	a		b		c		d	
18.0	0.007	0.017	0.029	0.018	0.031	0.017	0.022	0.015
18.1	0.034	0.017	0.052	0.019	0.048	0.017	0.030	0.016
18.2	0.006	0.017	0.014	0.018	-0.007	0.017	-0.006	0.015
18.3	0.007	0.017	0.008	0.018	0.001	0.017	0.002	0.015
18.4	0.008	0.017	0.007	0.018	0.011	0.017	0.026	0.016
18.5	0.004	0.017	0.002	0.018	0.009	0.017	0.019	0.016
18.6	-0.002	0.017	0.012	0.019	-0.003	0.017	0.016	0.016
18.7	0.007	0.017	0.019	0.018	0.004	0.017	0.005	0.016
18.8	0.011	0.017	0.014	0.018	0.009	0.017	0.008	0.016
18.9	-0.014	0.017	-0.004	0.018	-0.011	0.016	-0.014	0.015
19.0	-0.012	0.017	-0.006	0.018	-0.009	0.017	-0.006	0.015
19.1	-0.009	0.018	-0.014	0.019	-0.007	0.017	0.006	0.016
19.2	0.005	0.018	0.003	0.019	-0.010	0.017	0.009	0.016
19.3	-0.008	0.018	0.007	0.019	-0.003	0.017	-0.005	0.016
19.4	-0.003	0.018	0.019	0.019	0.005	0.018	0.012	0.016
19.5	-0.011	0.017	-0.017	0.018	-0.010	0.017	-0.012	0.016
19.6	-0.030	0.017	-0.037	0.018	-0.013	0.017	-0.023	0.016
19.7	-0.031	0.017	-0.010	0.019	-0.017	0.017	-0.015	0.016
19.8	-0.005	0.018	-0.007	0.019	-0.017	0.017	-0.012	0.016
19.9	0.015	0.019	0.017	0.020	0.011	0.018	0.016	0.017
20.0	0.000	0.000	0.000	0.000	0.000	0.000	0.000	0.000

and $M(Q)$ is the simulated structure factor. The summations proceed over the measured data values. The new distribution is achieved by adding or subtracting a random number of atoms at each r value in turn. The acceptance of each move follows the usual rules of Metropolis Monte Carlo with a Boltzmann-like probability function,

$$p(\Delta R_f^2) \sim \exp(-\lambda \Delta R_f^2),$$

where ΔR_f^2 represents the change in R factor with the move and λ is a "temperature factor" which controls how close the simulation fits the data. Thus as λ is made larger the simulation attempts to fit the data with a smaller R factor. An additional constraint is also imposed on the distribution [in this case a constraint is placed on the second derivative of $N(r) = 4\pi\rho r^2 g(r)\Delta r$, where Δr is the

bin width] to ensure that the final distribution is as smooth as possible. In this way the calculated distributions are largely free from the bias associated with truncation and noise in the measured data. The results of this calculation are shown in Fig. 5. Note that these pair correlation functions are significantly above unity for r values out to 15 Å, an effect associated with the very-high-compressibility limit $S(0)$ under the present conditions (see Table I). Certainly the qualitative behavior of $g(r)$ is clear and can be used to draw some conclusions. The very pronounced peak at ~ 0.76 Å is associated with the intramolecular bond distance, while no simple explanation exists for the structure around 2.5 Å.

On the $T = 41.8$ K isotherm [curves (b), (c), and (d)] the height of the first peak, as well as its width, decreases with increasing density and a second maximum develops in the region around 7 Å. The general behavior of the radial distribution function with density appears normal and no unexpected additional structure is evident at the critical density. In particular the near-neighbor coordination numbers, integrated out to 5.1 Å, for the cases (b), (c), and (d), are 4.8, 6.2, and 7.6, respectively. We now attempt to make these considerations more quantitative by considering a classical simulation using a Lennard-Jones potential appropriate to deuterium to see in more detail what "normal" behavior should look like.

V. MONTE CARLO SIMULATION

We have performed a classical simulation of a monatomic Lennard-Jones system in thermodynamic conditions similar to that of the experiment. We are well aware that the comparison can be only qualitative as deuterium is not monatomic and is not even a classical system at such low temperatures. There are some reasons,

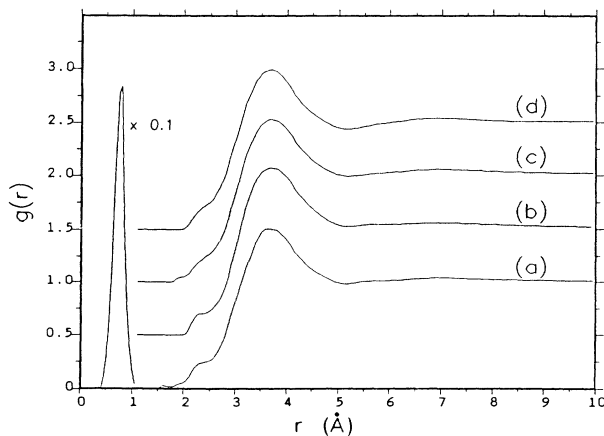


FIG. 5. Atom-atom pair distribution function as obtained from direct inversion of the experimental $S(Q)$. The labels are defined in Table I.

however, why the classical simulation of a monatomic system can be used in this case. It is well known that hydrogens behave as free rotors even in the solid phase.²⁰ It is therefore a good approximation to evaluate the center of mass (c.m.) distribution of gaseous deuterium by means of the simulation of a monatomic gas. The effects of the molecular shape can be added to the end of the calculation, by means of a simple correction procedure, as it will be shown in Sec. VI. Concerning the quantum effects on the distribution function, these were already evaluated¹¹ for LJ deuterium and were shown to be quite considerable in the present thermodynamic conditions. However, the aim of the present work is to decide whether or not anomalous behavior of the pair distribution function can be detected for deuterium in the critical region. Therefore, in comparing the simulation results and the experiment, we will examine only the qualitative evolution of the relevant functions with density and/or temperature and we will leave to a successive investigation the comparison on an absolute scale. For the same reasons, the potential used for the simulation was the simple 6-12 Lennard-Jones potential with $\sigma = 2.96 \text{ \AA}$ and $\epsilon/k = 36.7 \text{ K}$, which can give good qualitative information.²¹

In order to make the simulations in thermodynamic conditions similar to the experiment, we have scaled the experimental densities and temperatures onto the respective critical values and we have chosen similar conditions for the simulations. For an LJ system the reduced critical density is $\rho_c^* = \rho_c \sigma^3 = 0.35$ and the reduced critical temperature is $T_c^* = kT_c / \epsilon = 1.35$.²² We have simulated nine points (three densities and three temperatures) in the critical region such that temperatures were just above T_c^* and the middle density was exactly ρ_c^* . The exact thermodynamic parameters are reported in Table III. The simulation program was a standard Monte Carlo routine, with a cubic box and periodic boundary conditions. The number of particles used was 64 in all cases. This allowed evaluation of the radial distribution function up to about $(2.6-3.1)\sigma$, i.e., beyond the second peak ($\approx 2.2\sigma$) of the $g(r)$. After several thousand moves, needed to equilibrate the system, the statistical averages were evaluated. The configurations were sampled when all particles had been selected for a random move, and every simulation was averaged over 10 000 configurations. Figure 6(a) shows the density evolution of the radial distribution functions for the reduced temperature $T^* = 1.627$. The solid line shows the zero-density limit of $g(\rho, x)$, $g_0(x) = \exp[-\Phi(x)/kT]$, where $\Phi(x)$ is the pair intermolecular potential as a function of the reduced distance $x = r/\sigma$, while the dotted lines refer to the highest and

lowest simulated densities, $\rho^* = 0.25$ and $\rho^* = 0.45$, respectively. Figures 6(b) and 6(c) show the same results for temperatures $T^* = 1.465$ and $T^* = 1.384$, respectively. Although it is not apparent from the figure, we have noted that in all three cases there is a minimum of the peak value of the radial distribution function for $\rho^* = 0.35$ (critical density). At higher intermolecular distances the amplitude of the oscillations around $g_0(r)$ increase monotonically with density in qualitative agreement with the experimental results of Fig. 5 which, however, refer to the site-site correlation function. The coordination numbers integrated out to the same R_{\max} ($= 5.1 \text{ \AA}$) as the experimental ones for the three corresponding RDF's at $T^* = 1.465$ [Fig. 6(b)] are 5.6, 7.5, and 9.4 and correspond to reduced densities 0.25, 0.35, and 0.45, respectively. It will also be noted that the main peak in the simulated $g(r)$ narrows with increasing density in a similar manner to the experiment. Due to the small number of particles used in the simulation, we cannot extend the comparison with the experimental functions beyond the second peak of the $g(r)$.

In order to compare the simulation directly with the experiment, it is necessary to transform the simulated dis-

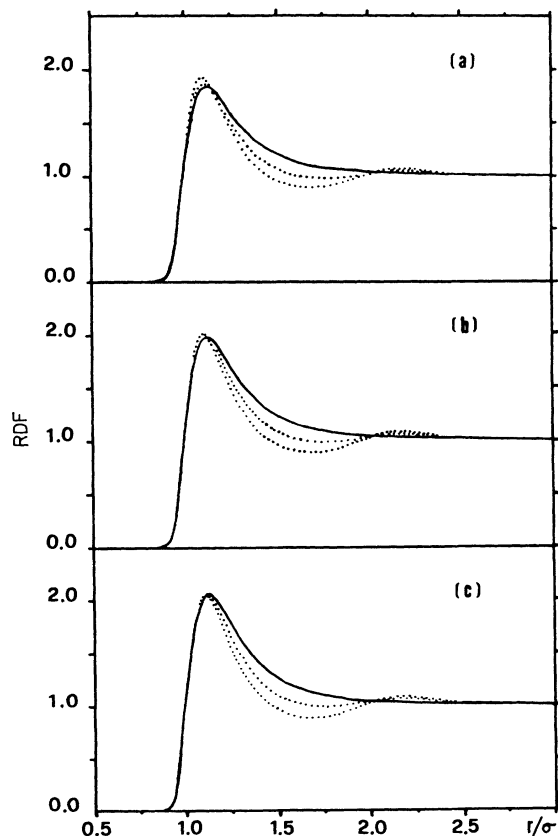


FIG. 6. Simulation results for the radial distribution functions at different reduced temperatures. (a) $T^* = 1.627$, (b) $T^* = 1.465$, (c) $T^* = 1.384$. The solid line represent the low-density limit $g_0(r)$, while dotted lines refer to the highest and lowest simulated densities $\rho^* = 0.25$ and $\rho^* = 0.45$ (see text).

TABLE III. Summary of the thermodynamic parameters used in the MC simulations. The critical parameters for a LJ system are $T_c^* = 1.35$ and $\rho_c^* = 0.35$ (Ref. 22). The LJ parameters for deuterium are $\sigma = 2.96 \text{ \AA}$ and $\epsilon/k = 36.7 \text{ K}$ (Ref. 21).

T^*	T^*/T_c^*	$T(K)$	ρ^*	ρ^*/ρ_c^*	ρ (molecules/nm ³)
1.384	1.025	39.3	0.25	0.714	7.46
1.465	1.085	41.6	0.35	1.000	10.44
1.627	1.205	46.2	0.45	1.286	13.42

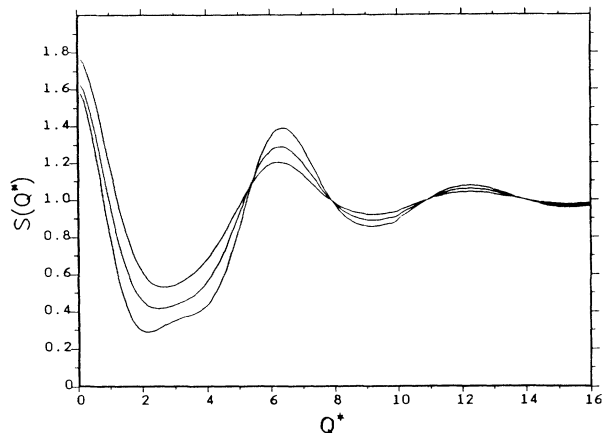


FIG. 7. Structure factor $S(Q^*)$ as obtained by Fourier transforming the simulated RDF at $T^*=1.465$. At low Q^* the behavior is monotonic with density while above $Q^*=5$ the oscillations increase regularly with ρ^* . The hump which appears in the region $Q^*=3-4$ is probably an artifact induced by the small size of the box used in the simulation.

tribution functions to Q space. The radial distribution function $g(r)$ can be Fourier transformed to give the static structure factor $S(Q)$, following the usual rule,

$$S(Q) = 1 + 4\pi\rho \int_0^\infty dr r^2 [g(r) - 1] \sin(Qr) / Qr. \quad (3)$$

The results for $T^*=1.465$ are reported in Fig. 7 as a function of the dimensionless variables $Q^*=Q\sigma$. In Q space a monotonic behavior with density of the overall c.m. functions is observed and the amplitude of the oscillations increases regularly with density for all three temperatures. The expected maximum of the compressibility, $S(Q=0)$, at the critical density (Table I) is not reproduced by the simulations, no doubt an artifact associated with the smallness of the box used in the calculations. The hump which appears at the highest density, in the region $Q^* \approx 3$, is also believed to be related to the same limitation. For these reasons the comparison with the experiment will be limited to the high- Q ($Q^* > 3$) region.

VI. DERIVATION OF THE MOLECULAR STRUCTURE FACTOR

The simulations produce the c.m. radial distribution function $g_c(r)$ and static structure factor $S_c(Q)$. However, the experiment measures the corresponding functions for the site-site correlations so that the c.m. functions from the simulation must be corrected for the molecular form factor in order to compare simulation with experiment. This task is easy for deuterium since the rotational motion of the molecule is believed to be uncorrelated with the translational motion, even in the solid phase.²⁰ Following Egelstaff *et al.*,²³ if we assume that for deuterium the molecular orientations of neighboring molecules are totally uncorrelated with each other and with the c.m. distribution, then the site-site scattering function can be written in the form

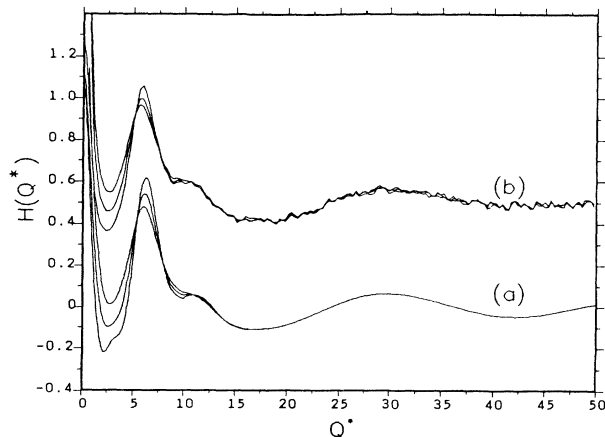


FIG. 8. (a) Corrected data for the "molecular" structure factor $S_m(Q^*)$ at $T^*=1.465$. (b) Experimental structure factor, plotted as a function of (Q^*) for $T=41.8$ K.

$$H(Q) = S(Q) - 1 = f_1(Q) + f_2(Q)[S_c(Q) - 1], \quad (4)$$

where $S_c(Q)$ is the c.m. static structure factor and the molecular form factors $f_1(Q)$ and $f_2(Q)$ are defined by

$$f_1(Q) = \frac{1}{2} [\sin(Qd) / Qd] \quad (5)$$

and

$$f_2(Q) = [\sin(Qd/2) / (Qd/2)]^2, \quad (6)$$

where d is the bond length of the deuterium molecule. These results assume a rigid molecule which is a reasonable approximation for deuterium over the Q range of interest.

Equation (4) can be used to correct the c.m. results, obtained from the simulation, for the molecular form factors. As it appears from Eq. (4), the zeros in $f_2(Q)$ preclude direct deconvolution from the data. Figure 8(a) shows the molecular $S_m(Q^*)$, as derived from the simulation data, after applying the correction procedure outlined above. The data are relative to $T^*=1.465$ ($T=41.6$ K) and the bond length $d=0.767$ Å was assumed. As a comparison we have plotted in Fig. 8(b) the experimental structure factors, as a function of (Q^*) , for the isotherm $T=41.8$ K. The similarity between the simulation and experimental results is striking, especially if we consider the approximations used in the calculations and the crudeness of the spherical LJ potential. In any case, from the comparison, no anomalous behavior of the experimental data can be detected. The behavior of the static structure factor of gaseous deuterium near the critical region seems normal and qualitatively predictable, even with a classical simulation.

VII. CONCLUSION

In conclusion we can state that, as far as the static structure of deuterium is concerned, the present experiment does not show any evidence for enhanced ordering near the main peak of the pair distribution function and

that its width monotonically decreases, as density increases, as is expected to happen for a classical monatomic system under the same thermodynamic conditions. The explanation of the peculiar effect measured by Raman scattering has to be sought, therefore, in some other phenomenon which affects the dynamical properties of gaseous critical deuterium, but whose equilibrium average is either zero or almost vanishing. Further work to study the size of quantum effects in the measured distribution functions and structure factors is in progress.

ACKNOWLEDGMENTS

We would like to thank the Science and Engineering Research Council (U.K.), the Consiglio Nazionale delle Ricerche (Italy), and the Fondazione Angelo Della Riccia (Italy) for funding this collaboration, I. F. Bailey, B. C. Boland, and the Sample Environment Group of ISIS in general, for technical assistance during the preparation of the experiment.

-
- ¹A. Teitsma and P. A. Egelstaff, *Phys. Rev. A* **21**, 367 (1980).
²P. A. Egelstaff, A. Teitsma, and S. S. Wang, *Phys. Rev. A* **22**, 1702 (1980).
³P. Loubeyre, *Phys. Rev. Lett.* **58**, 1857 (1987).
⁴J. A. G. Powles and J. L. F. Abascal, *J. Phys. C* **16**, 441 (1983).
⁵D. Thirumalay, E. J. Bruskin, and B. J. Berne, *J. Chem. Phys.* **79**, 5063 (1983).
⁶E. L. Pollock and D. M. Ceperley, *Phys. Rev. B* **30**, 2555 (1983).
⁷D. Thirumalay, R. W. Hall, and B. J. Berne, *J. Chem. Phys.* **81**, 2523 (1984).
⁸F. Barocchi, M. Zoppi, and M. Neumann, *Phys. Rev. A* **29**, 1331 (1984).
⁹F. Barocchi, M. Zoppi, and M. Neumann, *Phys. Rev. A* **31**, 4015 (1985).
¹⁰D. M. Ceperley and E. L. Pollock, *Phys. Rev. Lett.* **56**, 351 (1986).
¹¹F. Barocchi, M. Zoppi, and M. Neumann, *Phys. Rev. A* **36**, 2440 (1987).
¹²M. J. Clouter, C. G. Deacon, and H. Kieft, *Phys. Rev. Lett.* **58**, 1116 (1987).
¹³M. Zoppi, R. Magli, W. S. Howells, and A. K. Soper, *Physica B* (to be published).
¹⁴H. M. Roder, G. E. Childs, R. D. McCarty, and P. E. Angerhofer, National Bureau of Standards Technical Note No. 641 (unpublished).
¹⁵P. A. Egelstaff and A. K. Soper, *Mol. Phys.* **40**, 553 (1980).
¹⁶J. A. Young and J. U. Koppel, *Phys. Rev. A* **33**, 603 (1964).
¹⁷V. F. Sears, *Proc. Phys. Soc.* **86**, 965 (1965).
¹⁸A. K. Soper and P. A. Egelstaff, *Nucl. Instrum. Methods* **178**, 415 (1980).
¹⁹A. K. Soper, in *Proceedings of the International Workshop on Static and Dynamic Properties of Liquids* (Dubrovnik, Yugoslavia, in press).
²⁰J. Van Kranendonk, *Solid Hydrogen* (Plenum, New York, 1983).
²¹J. P. Hansen and I. R. McDonald, *Theory of Simple Liquids* (Academic, New York, 1976).
²²J. J. Nicholas, K. E. Gubbins, W. B. Street, and D. J. Tildesley, *Mol. Phys.* **37**, 1429, (1979).
²³P. A. Egelstaff, D. I. Page, and J. G. Powles, *Mol. Phys.* **20**, 881 (1971).